Innovations in Space-Object Shape Recovery and 3D Space Debris Localization

S. Prasad
Univ. of New Mexico
(in collaboration with WFU group)

2016 SSA Workshop

Maui, HI

Sep 17, 2016

*Work supported by AFOSR

Outline

THE UNIVERSITY of NEW MEXICO

- Two major SSA thrust areas –

I. 3D shape recovery of reflecting objects from solar BRDF data – based on the
   - Spatial distribution of specular BRDF around glint points
   - Polarimetric processing to extract specular data

II. 3D localization of space debris in space-to-space imaging via optical vortex states
   - Rotating PSF imaging based on Bessel vortex states
   - Excellent transverse+range (3D) localization precision

- Statistical characterizations of estimation fidelity

Surface recovery via spectral polarimetric BRDF under solar illumination

- Mathematically smooth surfaces – BRDF has only isolated glint points (ideal reflection condition)

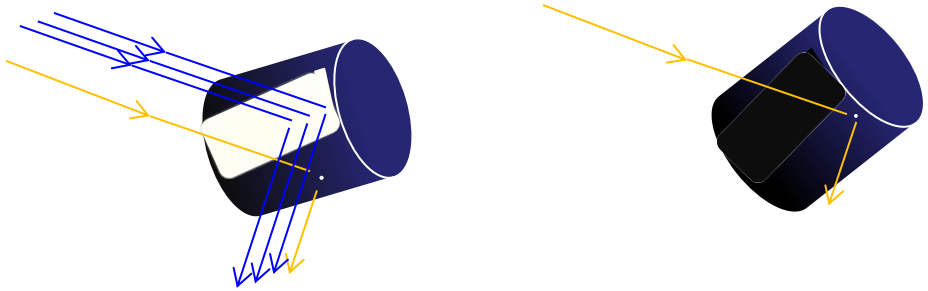

- Roughened (real) surfaces – glint spots/regions, 2D BRDF distribution characteristic of local 3D shape
  - Micro-roughened (man made) vs. naturally roughened/pitted – specular vs. diffuse
  - Color largely in diffuse BRDF - spectral analysis

Asteroid Ida, moon Dactyl

Polarimetric BRDF

- Incident sun light – unpolarized with Stokes parameters,

$$s_0^{(i)} = I_0, \quad s_1^{(i)} = s_2^{(i)} = s_3^{(i)} = 0$$

  - ➔ only need M_{i0} components,

$$\boxed{M_{00} = \tfrac{1}{2}(|r_s|^2 + |r_p|^2), \quad M_{10} = \tfrac{1}{2}(|r_s|^2 - |r_p|^2), \quad M_{20} = M_{30} = 0}$$

- Polarimetric BRDF (pBRDF): (Hyde *et al.*, Opt. Express, 2009)

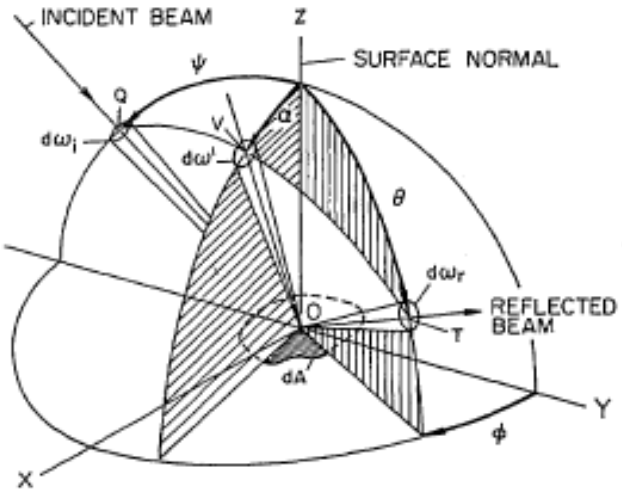

FIG. 1. Spatial angles of incident and reflected flux.

$$\boxed{\mathrm{pBRDF}_{\mu\nu} = \frac{dN_{\mu\nu}^{(r)}(\psi;\theta,\phi)}{N^{(i)}(\psi)\cos\psi\, d\omega_i} \sim M_{\mu\nu}}$$

Reflected Stokes-vector fraction,

$$\begin{pmatrix} s_0^{(r)} \\ s_1^{(r)} \\ s_2^{(r)} \\ s_3^{(r)} \end{pmatrix} = \frac{P(\alpha;\sigma_h)\, G(\psi,\theta,\phi)}{4\cos\psi\, \cos\theta\, \cos\beta} \begin{pmatrix} M_{00} \\ M_{10} \\ M_{20} \\ M_{30} \end{pmatrix}$$

Specular vs. Diffuse Component

- Diffuse component – from part of reflected/transmitted fraction that is multiply scattered in the surface layers

- Specular fraction – singly reflected, partially polarized, specular component

- Spectral signature – contained in the spectral dependences of
  * singly reflected power (largely white); and
  * multiply reflected, diffuse power ("material color")

- Difference polarization data would reveal only specular component and its surface shape / texture dependence!

Roughness Models and Geometrical Primitives

- Microfacet model – very popular in comp. graphics
  - surface imperfections are planar facets ("μ-facets")

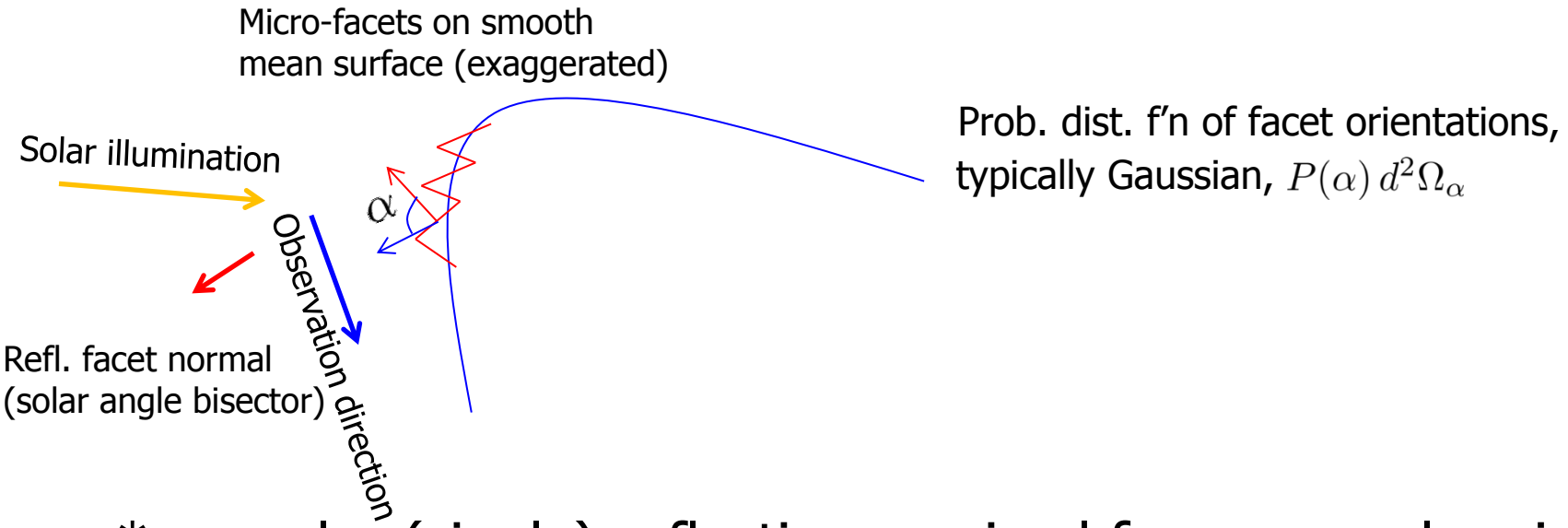

* specular (single) reflection received from properly oriented μ-facets only
* roughness primitives are planes, but can be extended to curved ones, e.g., pitted surface

Surface Characterization

- Low-dimensional global parameterization, e.g.,
  - a 5-parameter superquadric (generalized quadrics)

$$\left[\left(\frac{|x|}{a_1}\right)^{2/\epsilon_2} + \left(\frac{|y|}{a_2}\right)^{2/\epsilon_2}\right]^{\epsilon_2/\epsilon_1} + \left(\frac{|z|}{a_3}\right)^{2/\epsilon_1} = 1$$

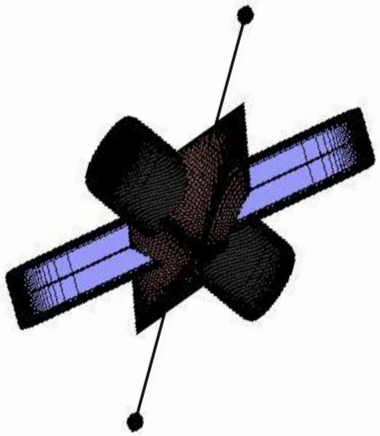

* satellite mock-up generated using five SQs

- Local (patch-by-patch) polynomial representation
  - Low-order bivariate polynomial, centered at $(x_o\ y_o)$,

$$z(x,y) = \sum_{n=1}^{N}\sum_{k=0}^{n} c_{k,n-k}(x-x_0)^k(y-y_0)^{n-k}$$

with order, N ~ 4-6

  - Stitch patches together for extended shape characterization

Polarimetric BRDF & Surface Recovery

THE UNIVERSITY of NEW MEXICO

- Premise - Geometry of 2D BRDF patterns on the sensor
  ➔ 3D surface shape around glint points

- Simulation model –
  - Surface geometry – a SuperQuadric
  - Surface roughness primitives – microfacets
  - Illumination/Observation – 2 illum. directions, 1 observ. direction
  - Noise models – Poisson and Gaussian additive
  - Parameters estimated –
  1. SQ approach – 5 size+shape, 3 Euler angles, 1 roughness (total 9)
  2. Polynomial patch recovery – N(N+3)/2 +1 parameters for Nth order polynomial (15-28 parameters for N=4-6)

- Global, non-convex recovery – fraught with local minima that prevent convergence of global optimizer to correct values

Our General Approach

THE UNIVERSITY of NEW MEXICO

- Two BRDF datasets needed for fully constrained recovery –
  - Each dataset yields a single angle for the normal at each surface point – need two polar angles to specify a normal
  - Spatial field of normals ➔ surface shape by integration
- Estimate the SQ surface from polarimetric BRDF data via *PatternSearch* global optimizer – fast, non-local
- Pre-optimize first on an ellipsoid – only 6 parameters – to constrain the glint points at which BRDF brightness is centered
  - Guarantees overlap of data estimate with actual data
- Impose low-order constraints on final optimization – glint point locations, CM and principal axes of thresholded BRDF data
- Alternating minimization – on fit-to-data and fit-to-low-order-constraints cost functions – prevents stagnation

Simulation Results for SQ Parametric Recovery

- General observations –
  - Initial step size in *PatternSearch* needs to be adjusted coarsely for success but it's all data based – expected value of fit-to-data (χ^2) is the guide!
  - Pre-optimizer must converge well – glint points on pre-op ellipsoid must match those in the actual datasets – for overlap needed to move the *PatternSearch* toward global min
  - Alternation of cost function from fit-to-data to fit-to-constraints is essential for constraint-guided global minimization of fit-to-data (χ^2) cost function
  - For moderate blurs, the larger the blur width the higher the success rate of convergence on different data frames – due to improved overlap of starting data estimate and actual data

SuperQuadric Shape Fitting - Results

- Surface parameters – $(a_1, a_2, a_3, \epsilon_1, \epsilon_2, \alpha, \beta, \gamma)$
- Two examples shown here

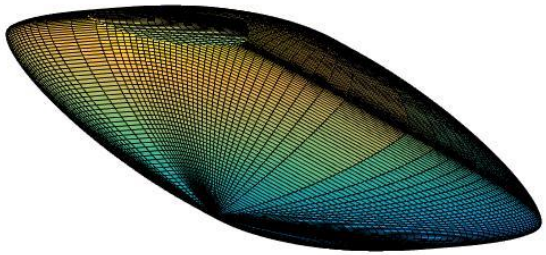

$(4, 2.5, 2, 1.5, 0.5, 2, 1, 1)$

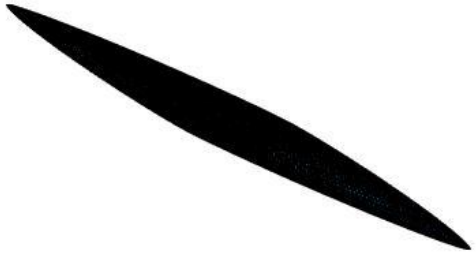

$(4, 1, 0.5, 1.5, 1.5, 2, 1, 1)$

- Results obtained for rounded vs needle shaped surfaces

- Results for a single data frame –
  - Convergence of alternating minimization – top points are fit-to-data CF values, bottom points constrained-based CF values

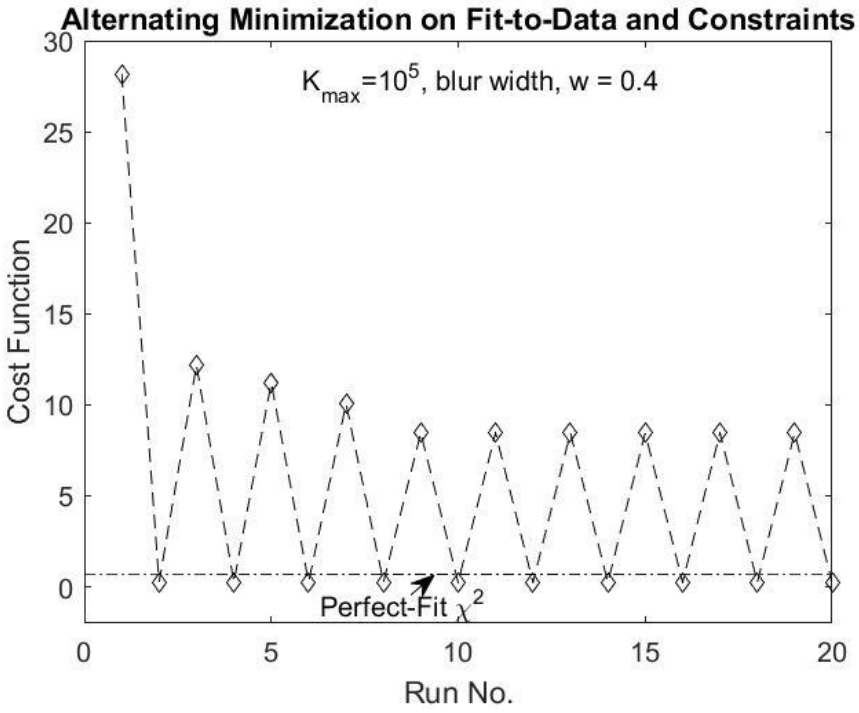

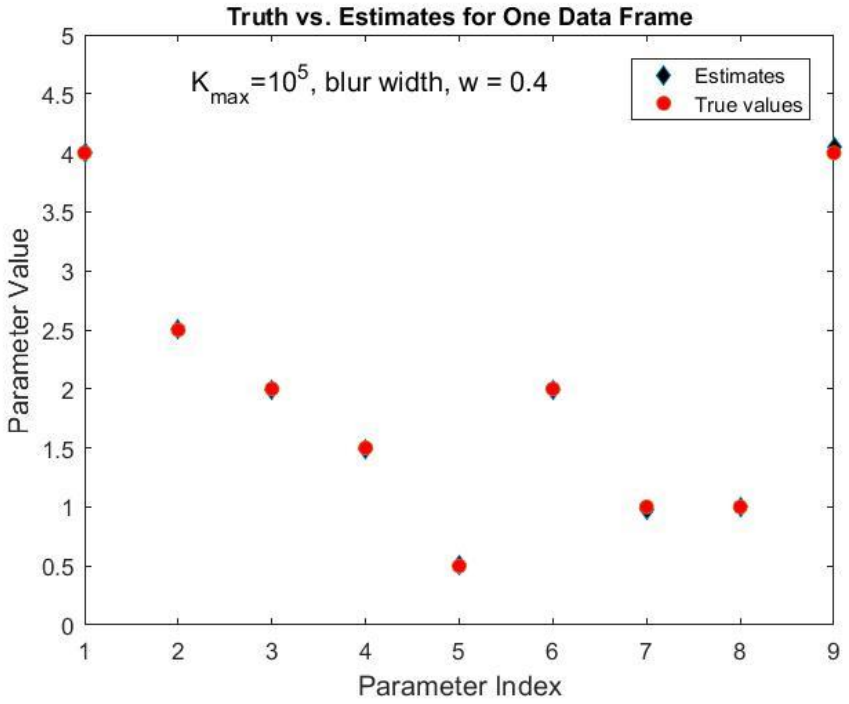

  - Parameters 1,2,3 – semi-axis lengths; 4,5 – shape parameters; 6,7,8 – Euler angles; 9 – surface roughness
  - Some failure (< 10-20 %) of convergence on needle-shaped surfaces

- Results for multiple data frames –
  - 10x2 frames of Poisson data for needle-shaped SQ surface
  - Frame-1 recovery – BRDF estimate (for solar half angle = 0.6 rad)

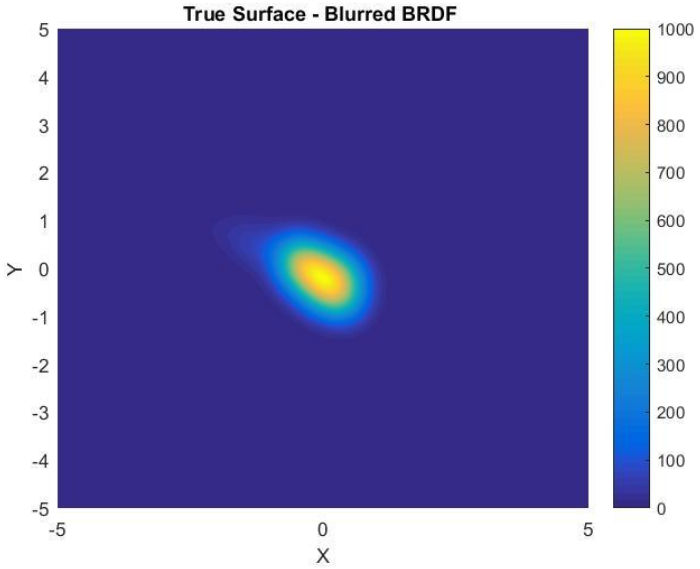

True Blurred BRDF

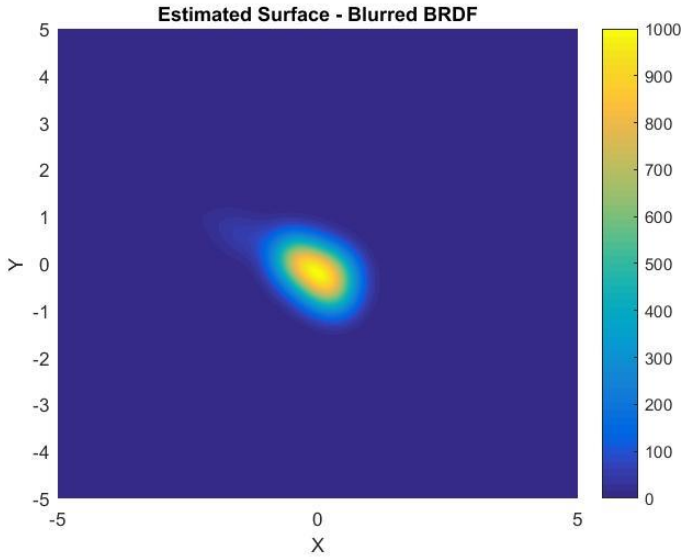

Estimated Blurred BRDF

Sensor Plane Data

- Blur width = 0.4
- True parameter values - $(4, 1, 0.5, 1.5, 1.5, 2, 1, 1, 4)$
- Blurred BRDF data well estimated in spite of poor estimate of a_1

- 10x2 frames of Poisson data for needle-shaped SQ surface
  - Recovery of parameter values (all 10 frames)

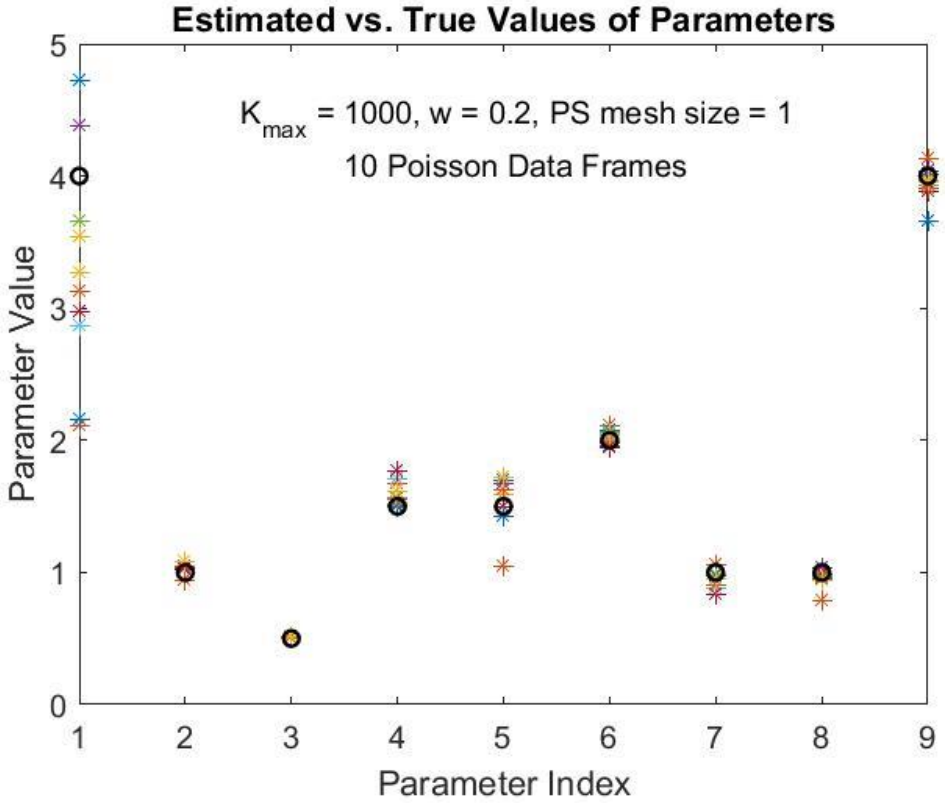

  - True parameter values - $(4, 1, 0.5, 1.5, 1.5, 2, 1, 1, 4)$
  - a_1 determined poorly

- Results for Gaussian additive-noise data are very similar

Polynomial Patch Shape Fitting

$$\left[\left(\frac{x}{a_1}\right)^{\frac{2}{\varepsilon_2}}+\left(\frac{y}{a_2}\right)^{\frac{2}{\varepsilon_2}}\right]^{\frac{\varepsilon_2}{\varepsilon_1}}+\left(\frac{z}{a_3}\right)^{\frac{2}{\varepsilon_1}}=1$$

$$a_1 = a_2 = 2, a_3 = 1, \varepsilon_1 = \varepsilon_2 = 1.2, \chi = 6$$

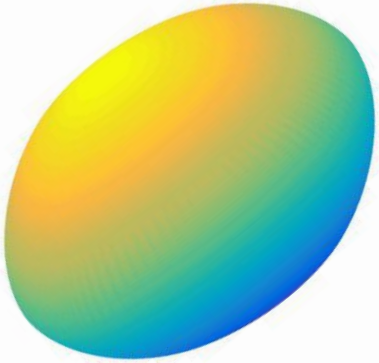

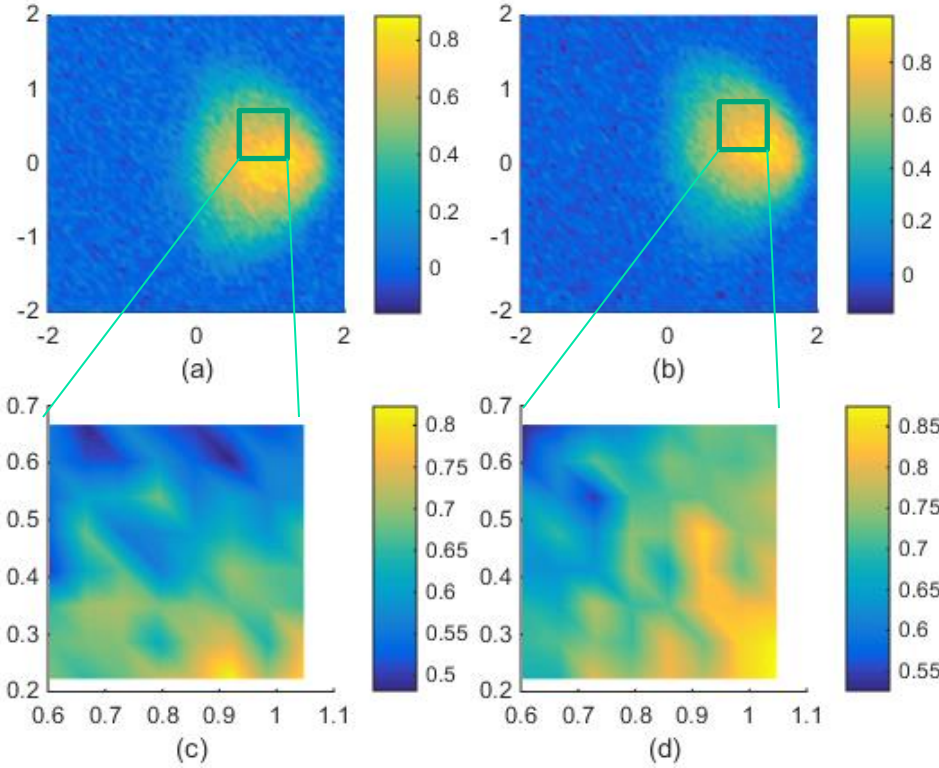

** 2 BRDFs from 2 illumination directions*

* Gaussian blur –
window size=5, sigma=3

* Additive Gaussian noise PSNR=20

* A fixed 8x8 patch cut out from the two images

** 4th order polynomial with 14 shape coefficients, 1 roughness parameter χ*

➔ *15 parameters to be estimated in all*

*Assume the 8×8 patch is centered in a 12×12 larger patch,
" yellow region" can be parameterized by same polynomial coefficients

*Blur the 12×12 BRDF with the given Gaussian filter (size $= 5, \sigma = 3$),
and cut out the 8×8 central part for data fitting

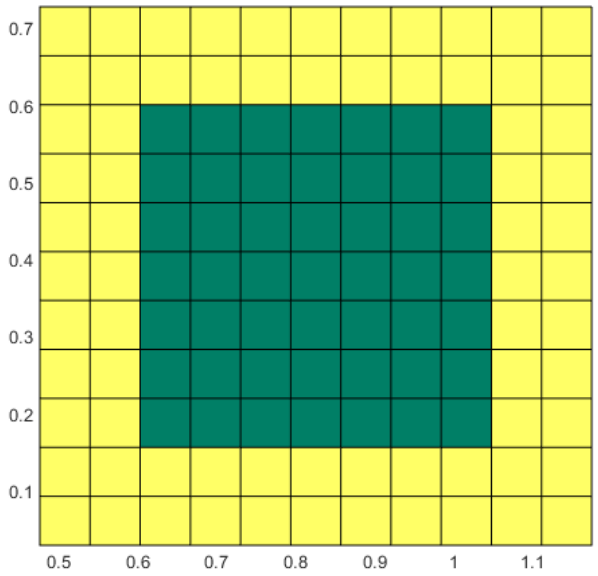

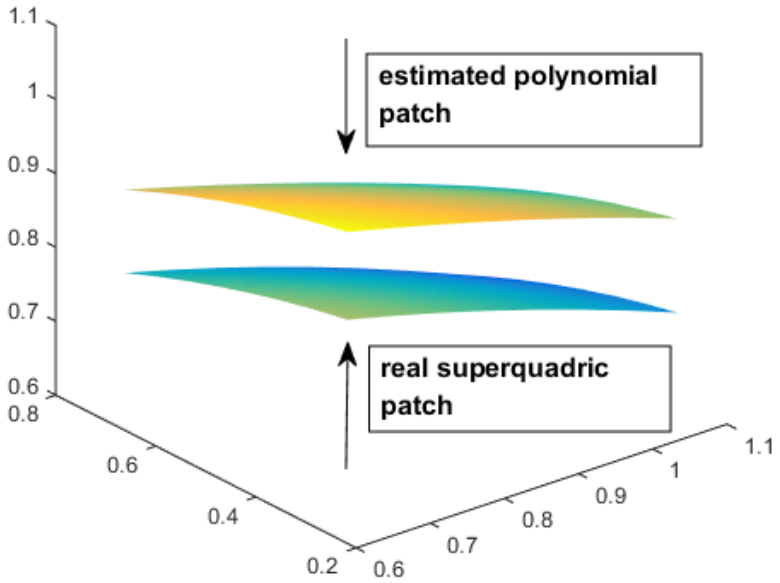

One reconstruction, additive Gaussian noise, PSNR=20

Result of patch shape recovery

Average shape error per pixel

$$E_{64} = \sum[(\hat{n}_x - n_x)^2 + (\hat{n}_y - n_y)^2]/64$$

E_{64} scatter plot vs PSNR (semi-log)

(500 realizations)

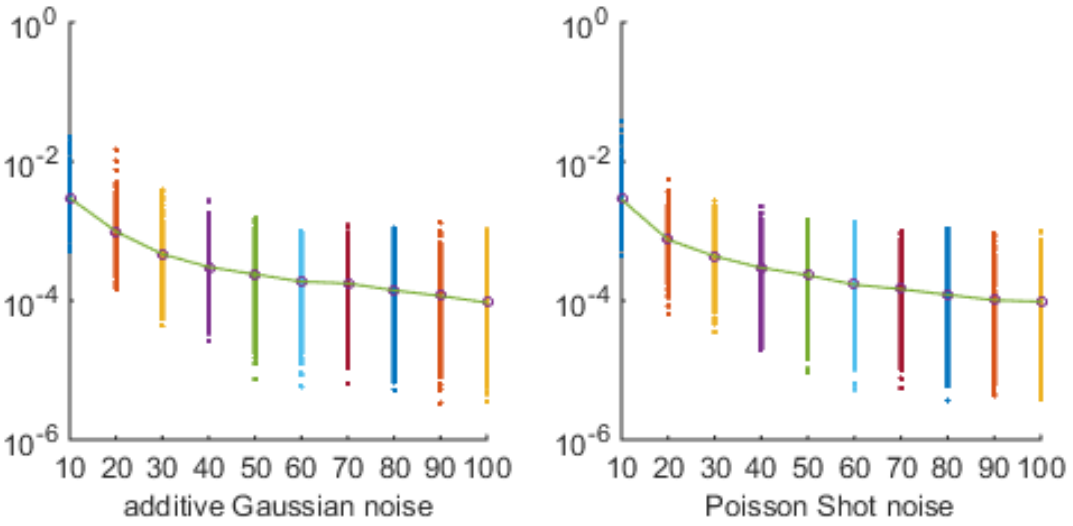

Inner 36 pixels are better estimated than outer 28 pixels as shown.

Polynomial approximation is better for smaller patch.

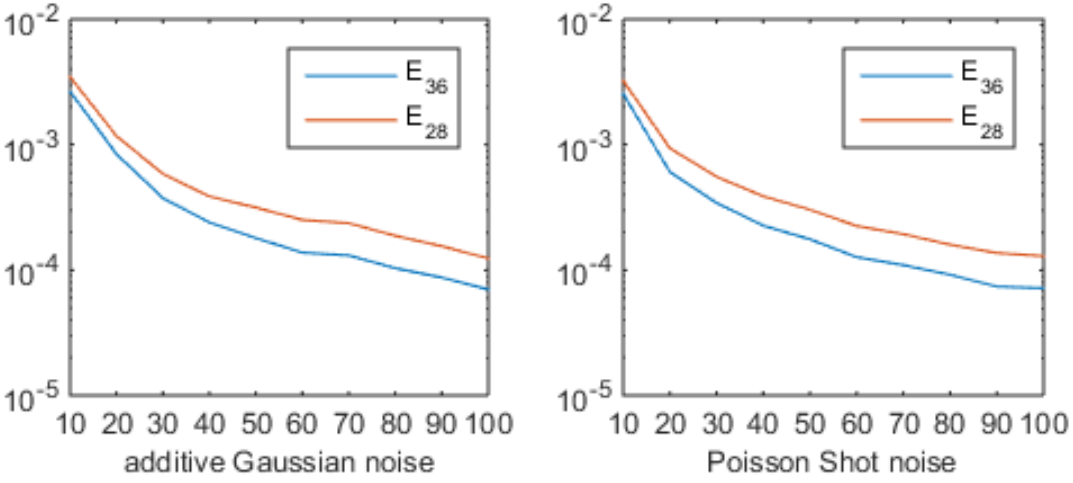

Mean over 500 realizations

Compare recovered polynomial coefficient with the "ground truth" coefficient (the best 4th order polynomial approximation of the *superquadric patch*)

$$z(x,y)=\sum_{n=1}^{4}\sum_{k=0}^{n}c_{k,n-k}\left(x-x_0\right)^k\left(y-y_0\right)^{n-k}$$

$$d_{k,n-k}=c_{k,n-k}L^n \qquad L=x_0-x_{\min}$$

Normalized coefficients, can be compared across orders

Squared error per normalized coefficient:

$$E_d=\sum_{n=1}^{4}\sum_{k=0}^{n}(d_{k,n-k}-\hat{d}_{k,n-k})^2/14$$

Squared error per normalized coefficient in each polynomial order:

$$E_d(n)=\sum_{k=0}^{n}(d_{k,n-k}-\hat{d}_{k,n-k})^2/(n+1)$$

Mean evaluated over 500 realizations, n=1,2,3,4,

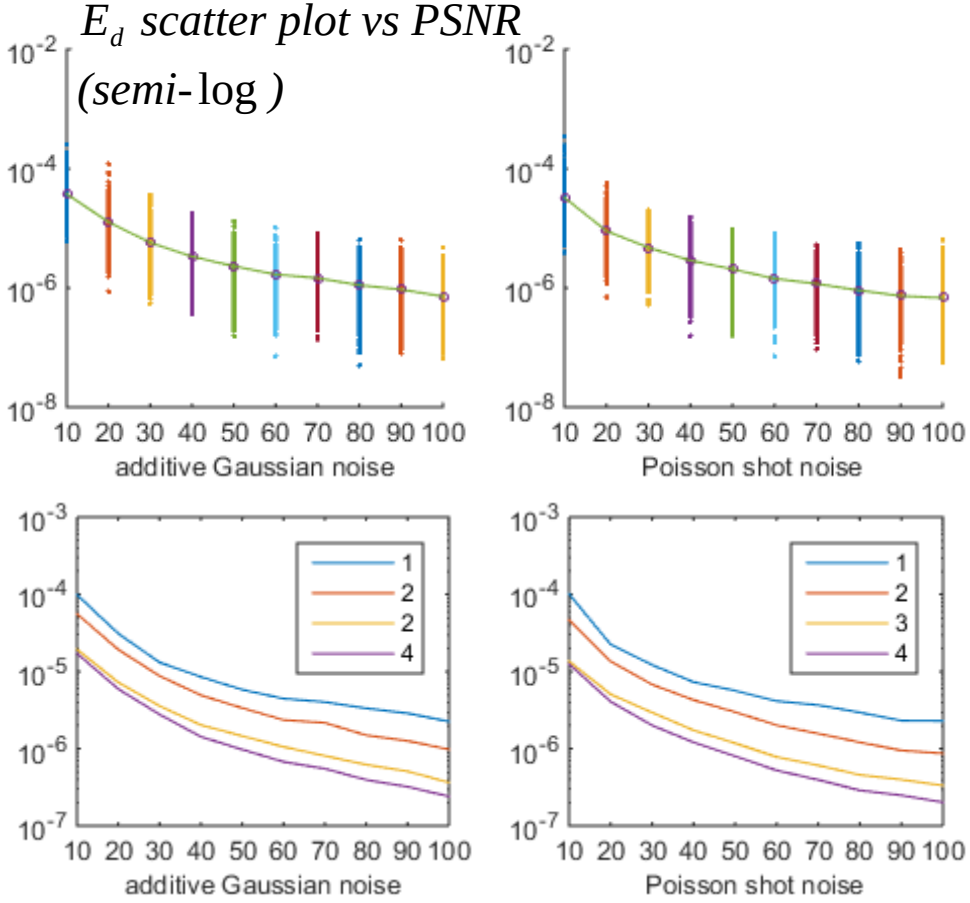

Conclusions (Part I – 3D surface shape recovery)

- Reliably reproducible results for SQ recovery via a novel alternating approach
- Use of pre-optimizer and physical constraints in an alternating algorithm seems critical to global min
- Two different views of the same object for unequivocal surface shape recovery
- Method generally applicable to general low-dimensional parametric surface models
- Polynomial patch recovery works well; needs to have a good starting value of the coeffs for success

Part II

Image Rotation and 3D Debris Localization

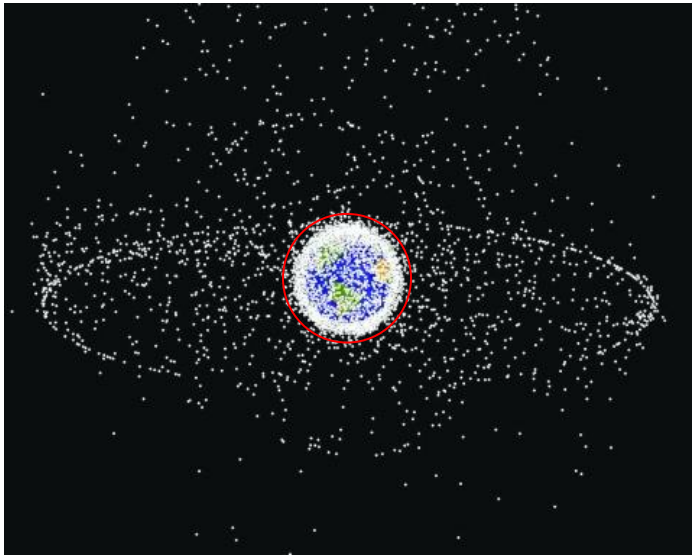

Space junk map
(courtesy of NASA)

LEO

- USAF Space Fence Solution – constellation of phased-array S-band radars across the globe to detect, track, and catalog LEO debris > 1.5Mx/day (Lockheed Martin lead)
- Combined radar-optical systems- for improved tracking across ranges (10's of km – 0.1 km)?

Turning an Optical Crank for Ranging

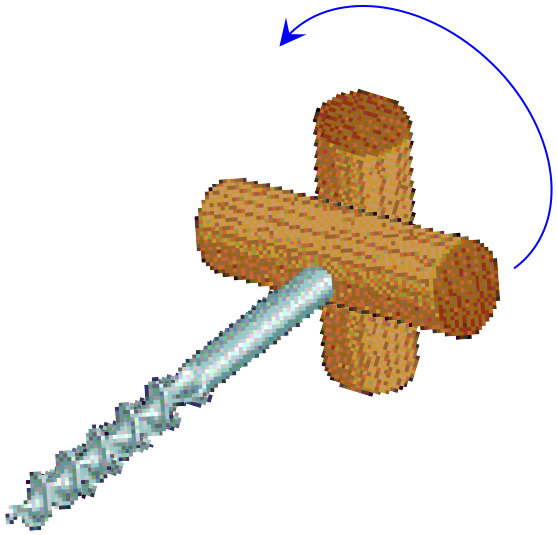

Rotating PSF Imagery

- Beam rotation with propagation via light angular momentum

- Superposition of vortex states – based on either
  - Gauss-Laguerre (GL) beams, or
  - Non-diffracting Bessel beams

  can create beam rotation with free-space propagation

- Use such rotation in an imager via pupil-phase engineering

– Fully transmissive mask

Sample LG Modes of Light

- $LG_m^n,\ n \neq 0,$ modes carry orbital angular momentum

- Intensity, phase, and Poynting vector for some low-order modes:

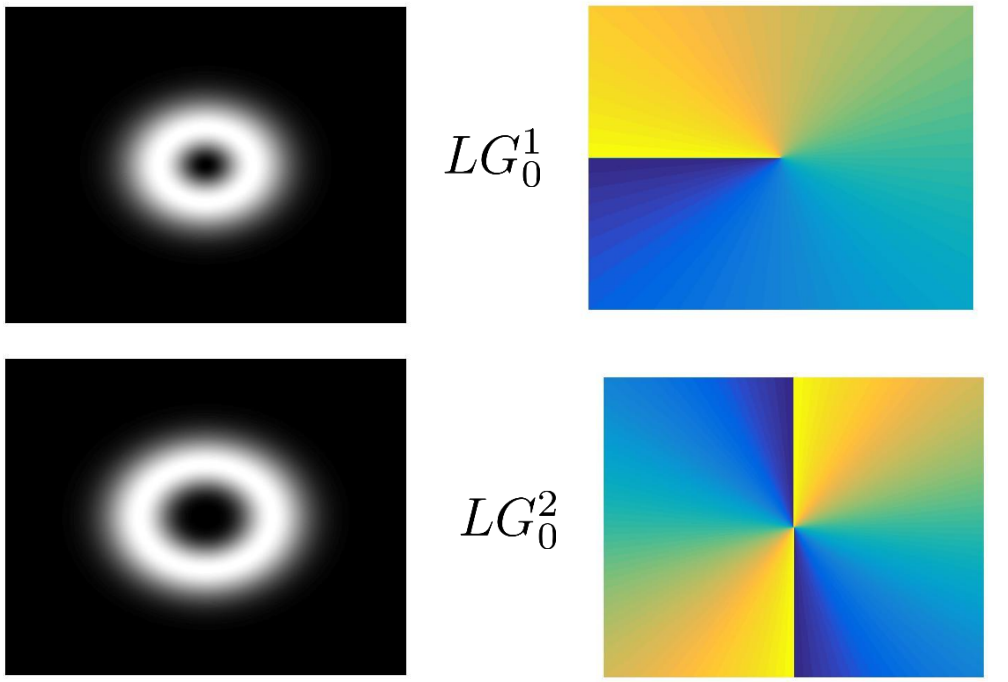

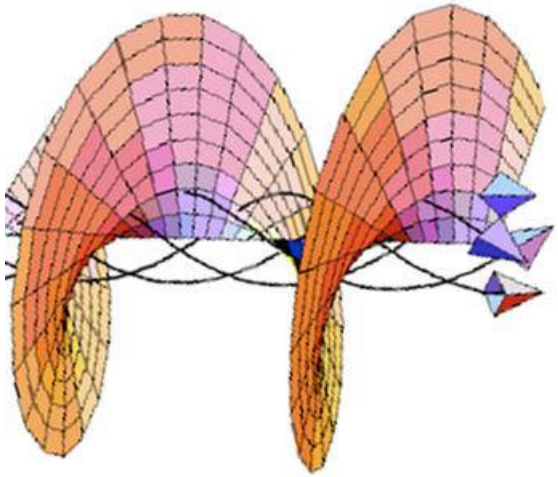

LG_0^1

Evans, Noe, Metcalf, MATLAB simulations

Experimental Realization of LG Beam

- Pass a plane wave through a computer generated hologram (CGH) that encodes the interference between a plane wave and a specific LG mode
- The emerging beam is that LG mode
- Superpositions of many LG modes may be similarly generated, with spatial separation among them if needed
- Spiral phase plates can also generate simple LG_0^n modes
- Design imager pupil with transmission function that is a superposition of appropriate LG modes ➔ PSF rotation

(R. Piestun, et al., 2006-present)

Bessel Vortex Beams

- Exact non-diffracting solutions of the scalar wave equation (no paraxial approx):

$$E(\vec{\rho}, z) = A(\vec{\rho})e^{i\beta z}, \;\; \beta < k_0$$

- Fourier representation – $A(\vec{\rho}) = \dfrac{A_0}{(2\pi)^2}\int ???\; e^{i\vec{k}\cdot\vec{\rho}}d^2k$
  - Answer – (k, ϕ, β) on a perfect cone of half angle $\tan^{-1}(\gamma/\beta)$

$$??? = \frac{1}{\gamma}\delta(k-\gamma)\, e^{\pm im\phi_k}, \;\text{with}\; \gamma^2 + \beta^2 = k_0^2$$

  - Amplitude has the form,

$$A(\vec{\rho}) \sim J_m(\gamma\rho)e^{\pm im\phi}$$

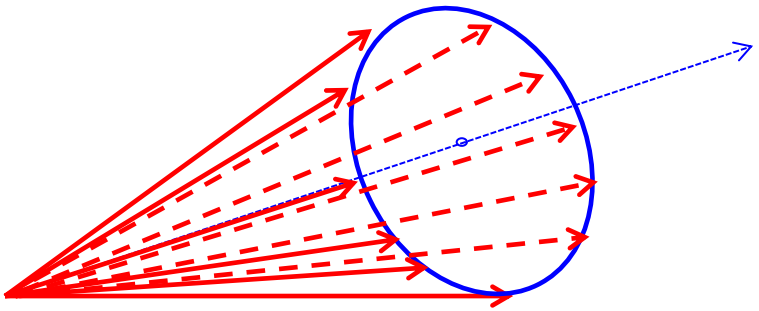

- Serious issue
  - Power is infinite, so impossible to generate in a lab
  - But approximate, largely non-diffracting Bessel beams can

Experimental Realization of Bessel Beams

- Pass an LG_0^n beam through an axicon ➔ n[th]-order Bessel beam

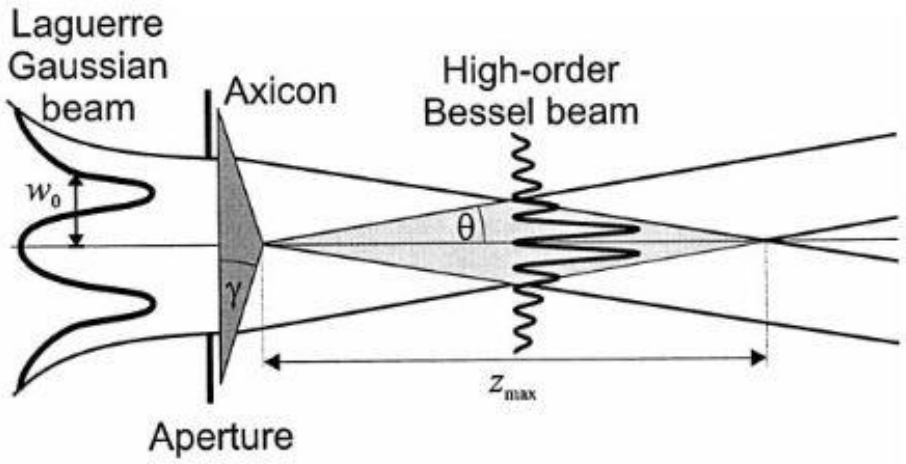

Arlt, Dholakia, Opt. Commun., 2000

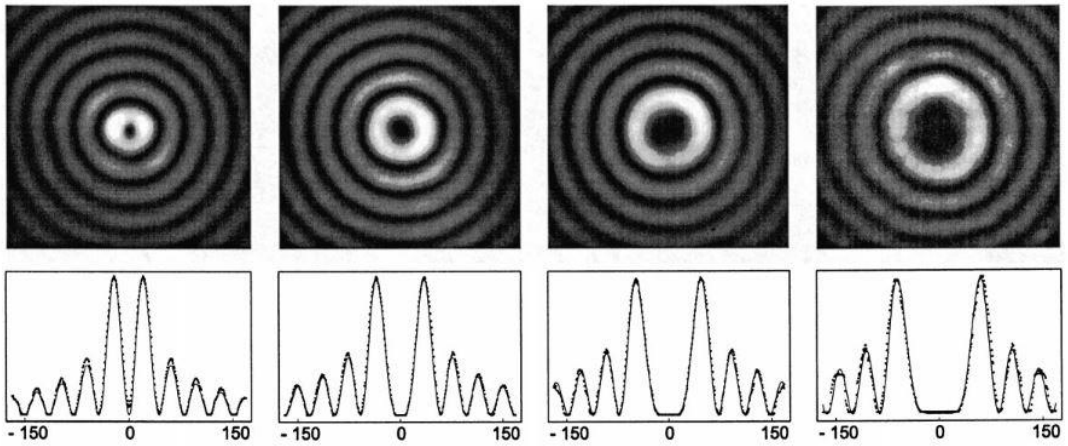

Fig. 2. Experimental beam cross-sections (355 μm × 355 μm) of Bessel beams of order $l = 1$ to 4 (from left to right) at a distance $z = 14$ cm behind the axicon. The radial profiles shown are the average of 40 azimuthal sections. They are in excellent agreement with the calculated profiles which are also shown. The radius of the inner ring increases with the order from $r_1 = 21.2$ μm to $r_4 = 61.2$ μm.

Rotating PSF w/ Bessel Beams

- Create beam spiraling via spiral phase mask

(Prasad, Opt. Lett.,'13)

  - Divide imaging pupil into Fresnel zones
  - m^{th} Fresnel zone carries $m\phi$ phase
  - Amplitude transmission function –

$$K(s,\phi_s,\zeta) \sim \sum_{m=1}^{M} e^{i\,m(\phi_s-\zeta/M)}\, J_m\left(2\pi\sqrt{m/M}\,s\right)$$

- PSF $|K|^2$ rotates w/ defocus ζ @ 1/M rad/defocus phase

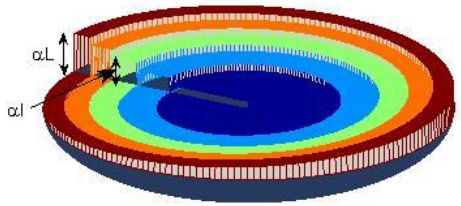

α = λ/(r-1)
λ: wavelength
r: index of refraction
l=1,2,..,L: zone index

Schematic of a 5-zone element (L=5)
(Color-coded for ease of visualization)

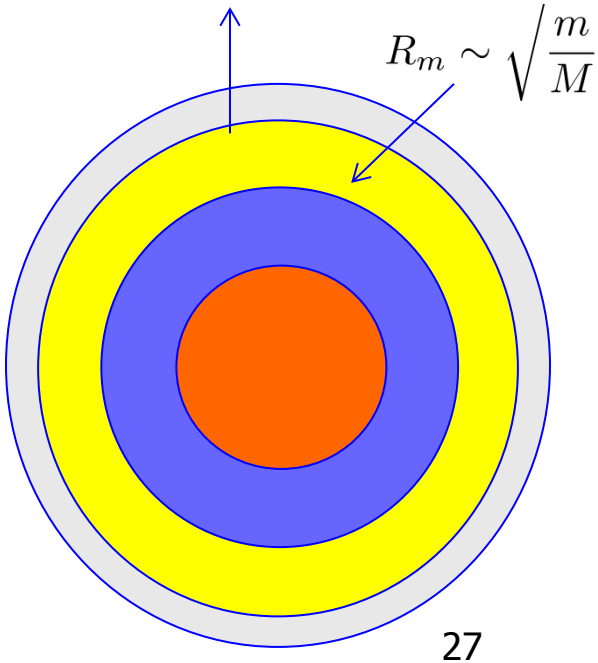

Depth of field vs. Transverse Resolution

- Perfect Bessel beams ➔ infinite depth of field
- Imperfect Bessel beams in imaging aperture due to finite-thickness cones in k space
- DOF limited by the number of zones, as their widths are controlled by it

  DOF $\propto M$
- But increasing M degrades transverse resolution ➔ optimal value of $M \sim$ 7-10

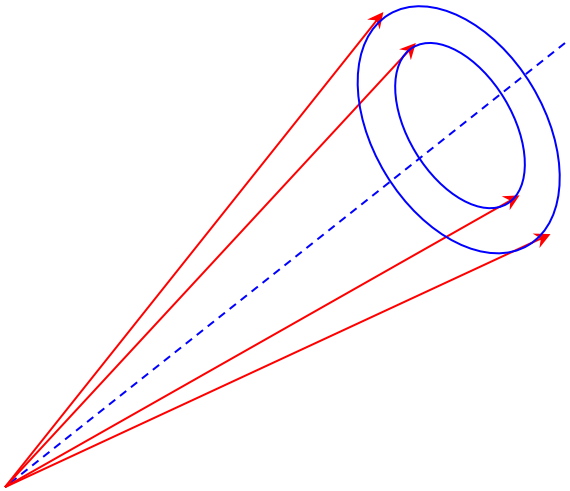

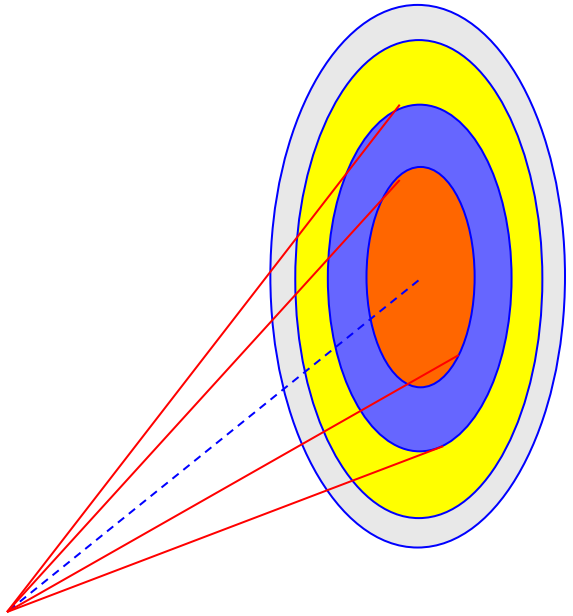

Single-Lobe Rotating PSF (M = 7)

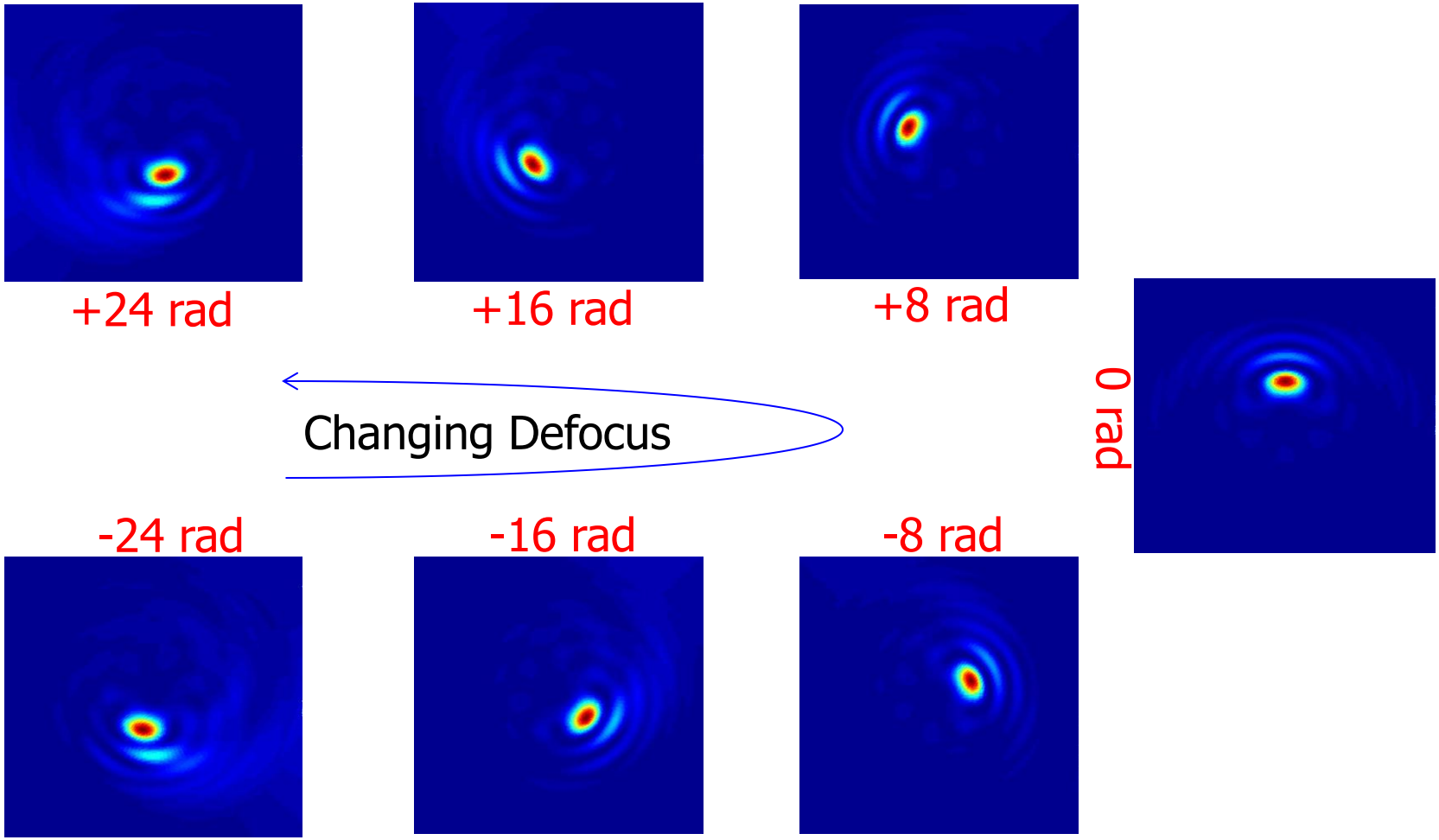

- One complete rotation over Δ (defocus) = $2M\pi$ radians
- Single-lobe PSF with relatively stable shape/size
- High 3D image capture/reconstruction sensitivity (cf. low-light levels)

Conventional PSF

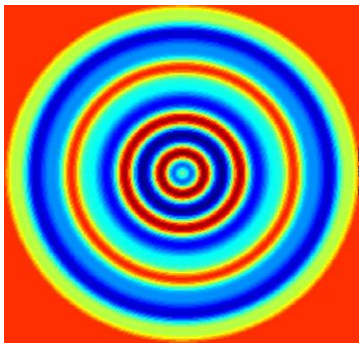

+24 rad

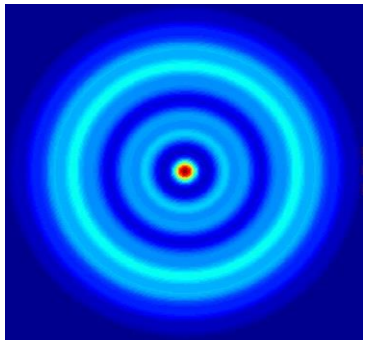

+16 rad

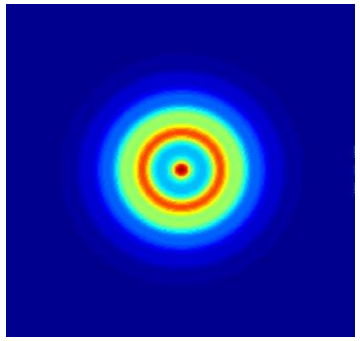

+8 rad

Changing Defocus

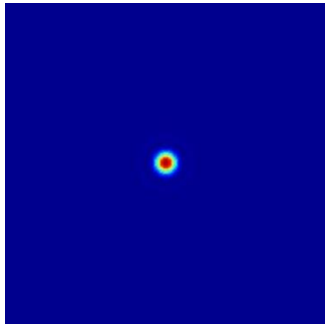

0 rad

-24 rad

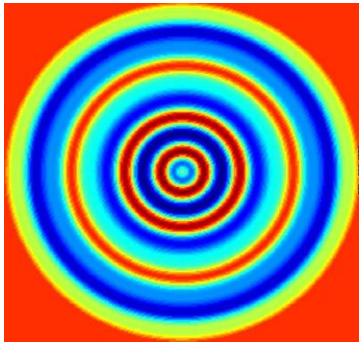

-16 rad

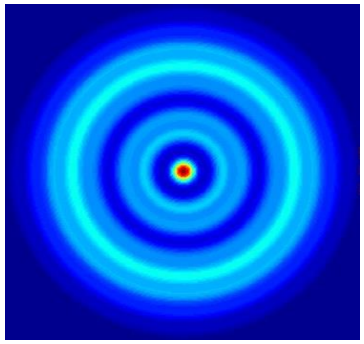

-8 rad

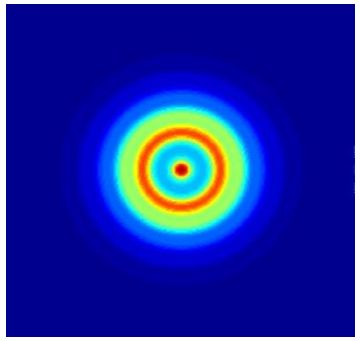

- Excellent in-focus 2D resolution (Rayleigh limit)
- High blur with increasing defocus – rapid loss of 3D resolution/sensitivity!

Dual-Use Imaging Technology

- Suitable for point-source localization microscopy and telescopic localization alike

- Differences –
  - High vs. low object-side NA; F# more relevant for telescopy
  - Source polarization and highly oblique rays require generalized, vector-field analysis in high-NA microscopy

    (Yu and Prasad, JOSA A, 2016)
  - Object distances are disparate ➔ linear vs. angular lateral localization

- Similarities -
  - Image rotation is the key property for z-localization!!

Space-Based Telescope for Debris Localization

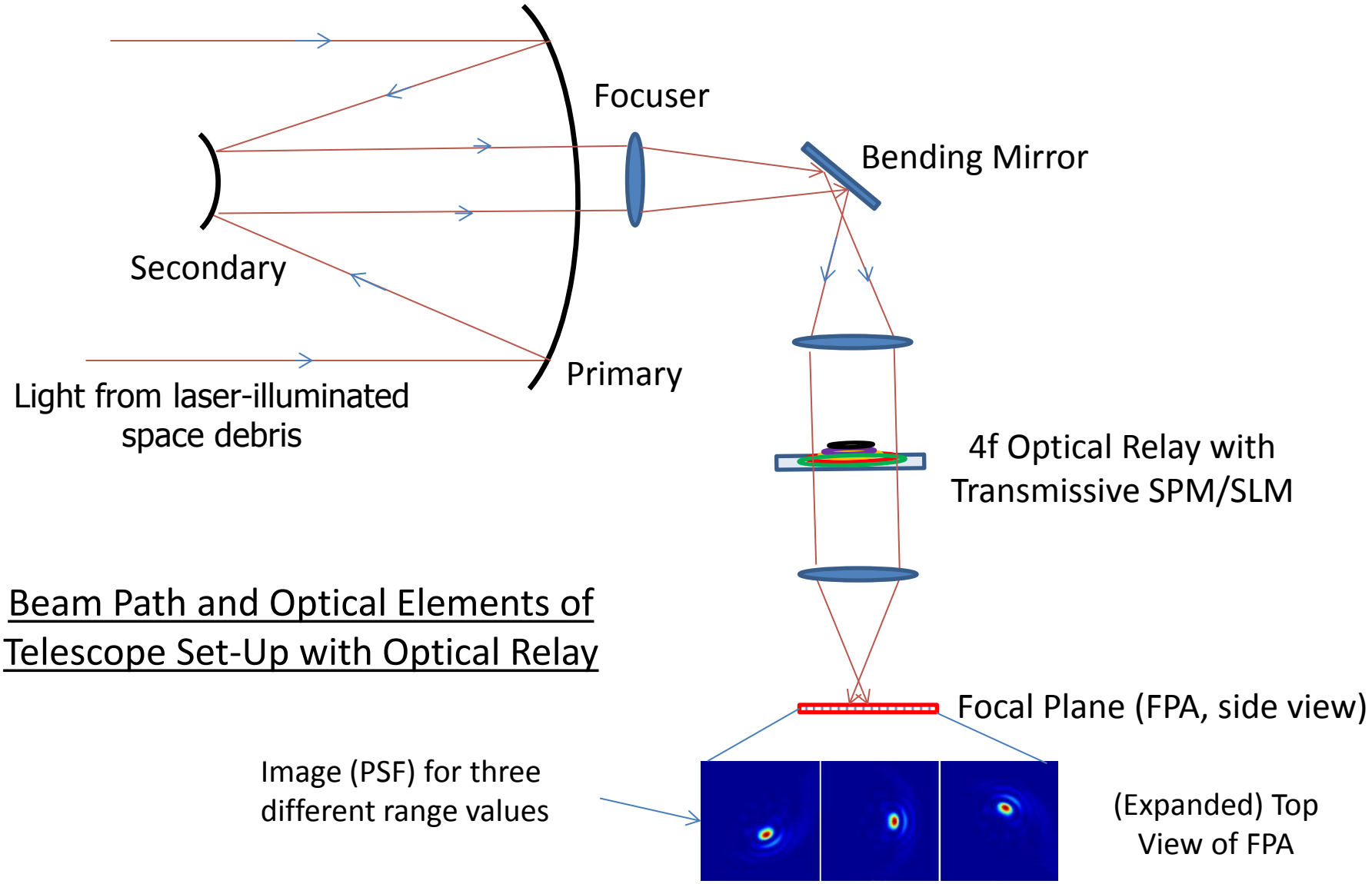

Beam Path and Optical Elements of Telescope Set-Up with Optical Relay

Minimum Resolvable Range (z)

- Everything is in focus sufficiently far
  - Maximum operational object range, $(z_O)_{max}$, is finite even at infinite brightness

- Minimum resolvable range,

$$\Delta\zeta_{min} = \frac{\Delta\zeta}{\Delta\phi}\Delta\phi_{min}$$
$$= M\Delta\phi_{min}$$

$$\Delta z_{min} = \frac{\Delta\zeta_{min}}{(d\zeta/dz)}$$
$$= (M\Delta\phi_{min})\,\frac{\lambda}{\pi}\left(\frac{z_O}{R}\right)^2$$

Range (z_O)	Δz_{min}
100 m	1.2 cm
500 m	30 cm
1,000 m	1.2 m
10,000 m	120 m

(R = 0.5 m, λ = 1 μm)

- Line-of-sight (LOS) sources resolved

Min. Resolvable Transverse (x,y) Separation

- Rotating PSF is extended by a factor 3-4 compared to Airy disk

- Min. resolvable separation,

$$\Delta r_{min} = 4\frac{\lambda z_O}{R} = 4\frac{\lambda}{\theta_O}$$

- Scales linearly with range (unlike range resolution)

Range (z_O)	Δr_{min}
100 m	0.8 mm
500 m	4 mm
1,000 m	8 mm
10,000 m	80 mm

(R=0.5 m, λ = 1 μm)

- Small minimum resolvable volume over a large 3D volume in a single snapshot (no need to refocus)
- Source localization accuracy is in fact much higher, depending on SNR

Results of Simulation

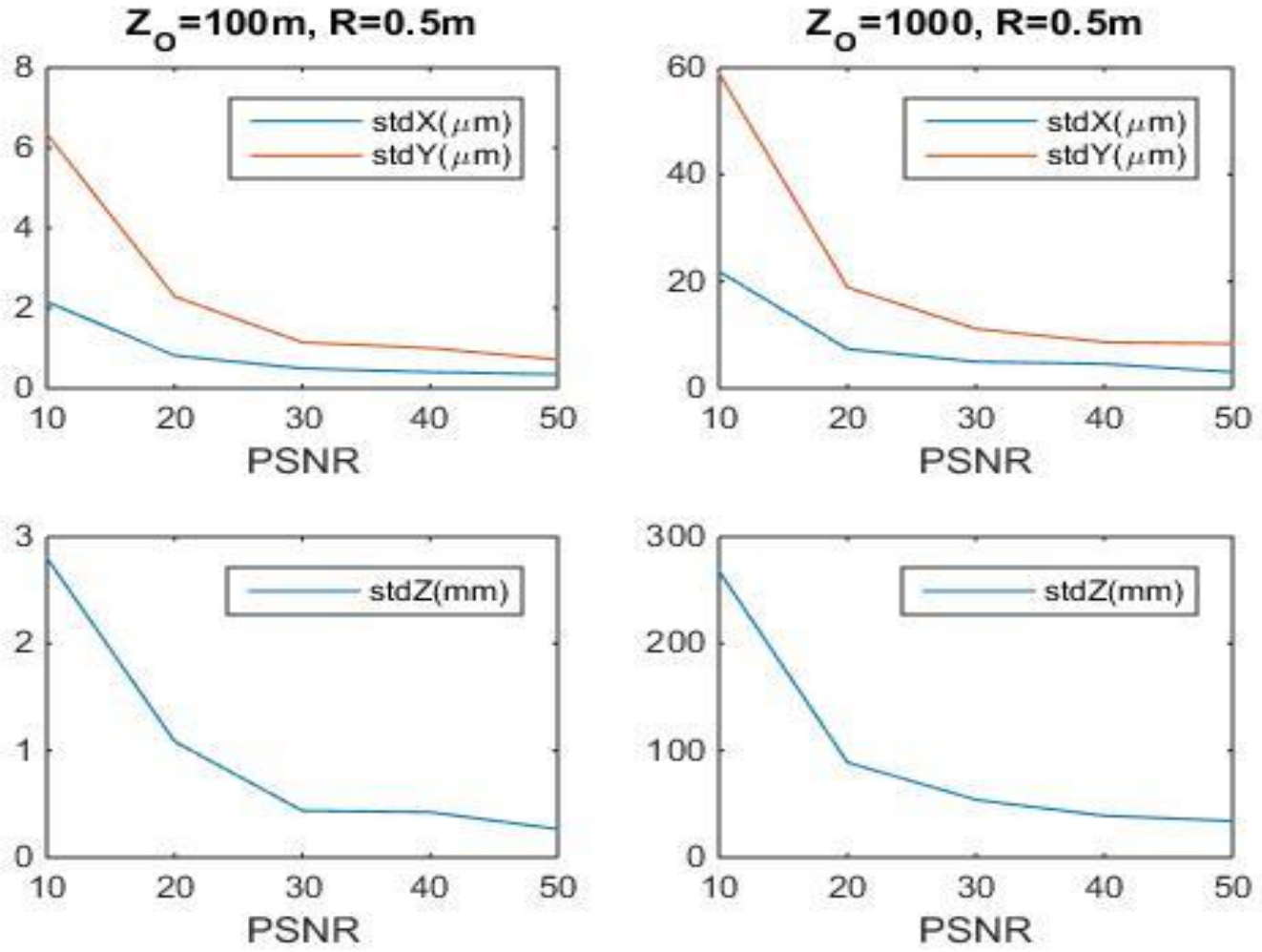

True location: X=0, Y=0, Z=Z_o

Illuminator Power Considerations

- Illuminate debris by either
1. rapidly sweeping collimated laser beams or
2. divergent ("conical") laser beams

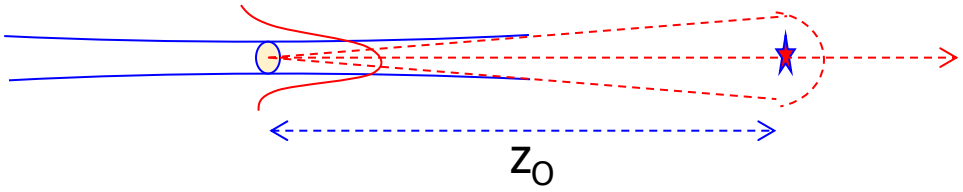

- Debris-scattered power scales as
  - Scattering cross-section, αA_d , $\alpha < 1$
  - Laser power, P_L
  - $1/z_0^2$ for collimated beam vs. $1/z_0^4$ for conical beam

Laser power needed for collimated Gaussian beam

Beam-center intensity:

$$I(\rho = 0, Z = Z_O) = \frac{1}{1 + (\frac{Z_O}{Z_R})^2} I_0, \qquad Z_R = \pi W_0^2/\lambda\text{: Rayleigh length}$$

$$(PSNR)^2 \frac{hc}{\lambda} = \frac{1}{1 + (\frac{Z_O}{Z_R})^2} I_0 \alpha A \frac{\pi R^2}{4\pi Z_O^2} M$$

$$P_L = \tfrac{1}{2}\pi W_0^2 I_o$$

$$\Rightarrow P_L = h\frac{c}{\lambda}(PSNR)^2 \frac{2\pi W_0^2 Z_O^2}{M\alpha A_d R^2}\left[1 + \left(\frac{\lambda^2}{\pi W_0^2}\right)^2 Z_O^2\right]$$

For $Z_O < Z_R$, $P_L \sim Z_O^2$

Power needed to achieve $PSNR = 10$

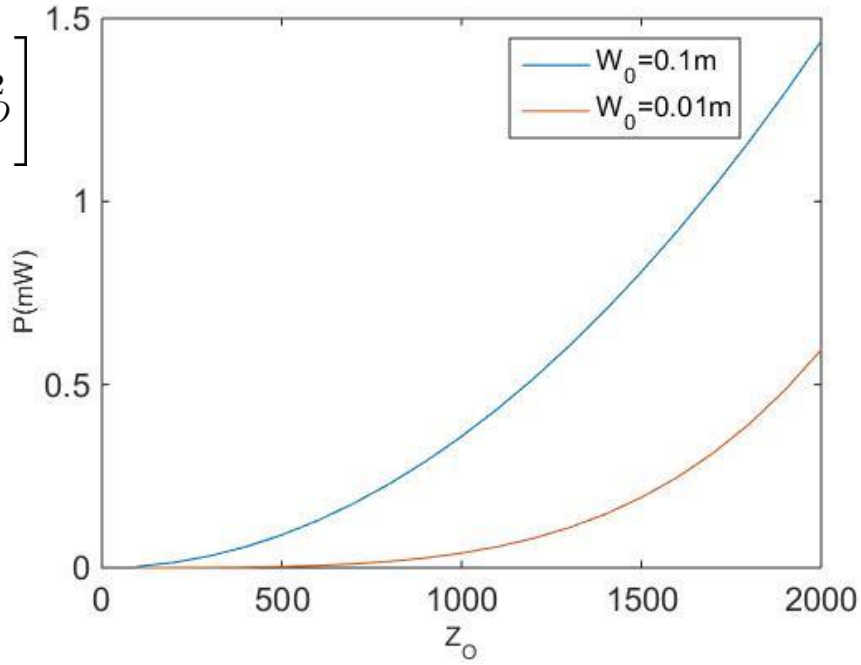

Laser power needed for divergent beam

$$P_L = (PSNR)^2 \frac{hc}{\lambda} \frac{1}{M} \frac{4\pi}{(\pi R^2/Z_O^2)} \frac{\Omega_L Z_O^2}{\alpha A_d}$$

$$\sim \frac{\Omega_L Z_O^4}{A_d A}$$

Ω_L: illuminator solid angle
A_d: cross-sectional area of the debris
αA_d: scattering cross-section
Z_O: object distance
R: aperture radius
M: peak image signal/total image sig

$\lambda = 1\mu m$
$M = 0.0279$ (pixel size=$\lambda Z_I/4R$)
α=0.5, $A_d = 1mm^2$, $R = 0.5m$

Power needed to achieve $PSNR = 10$

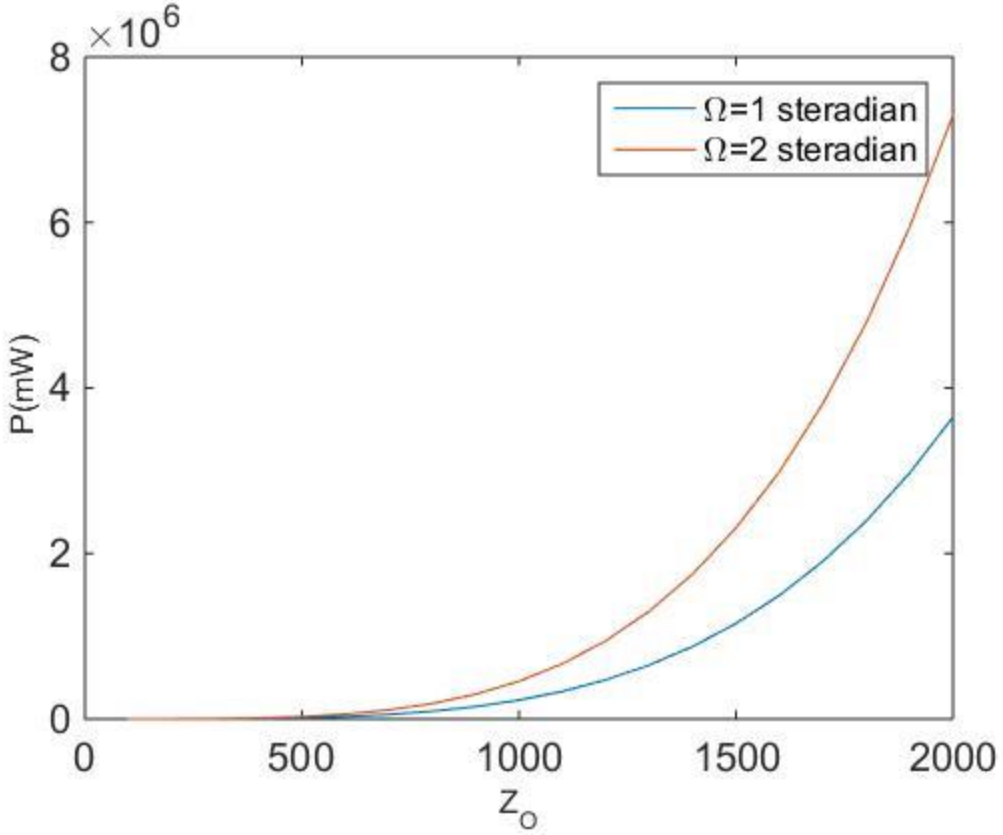

Multiple Debris in 3D FOV

- Realistic simulation of the imaging process relative to varying point source-telescope distances, optical and detector characteristics, and inherent Poisson noise

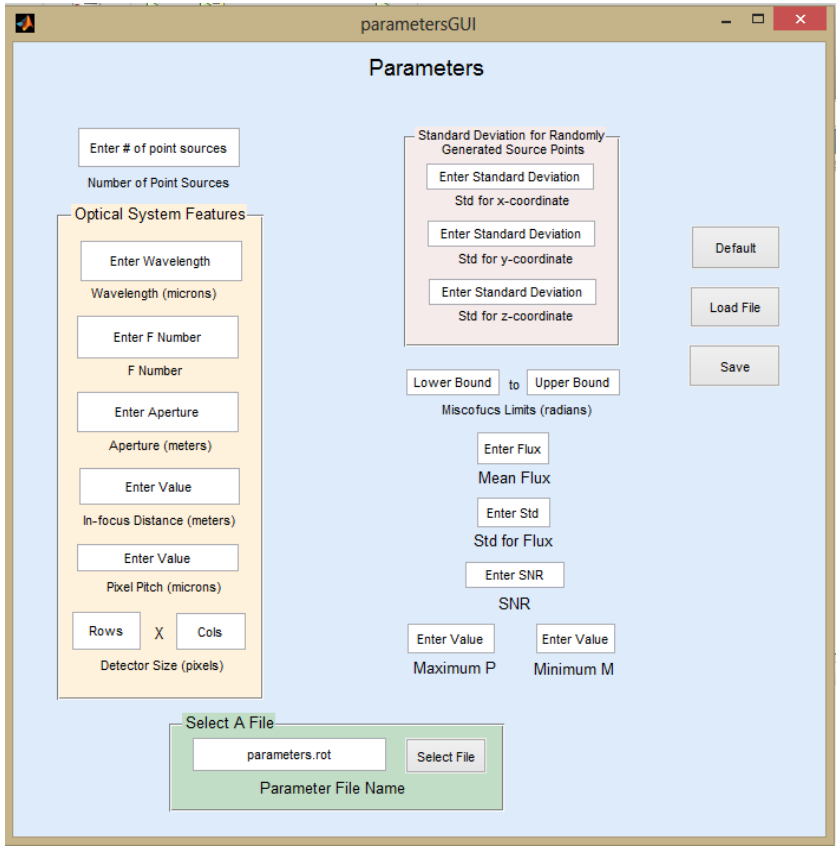

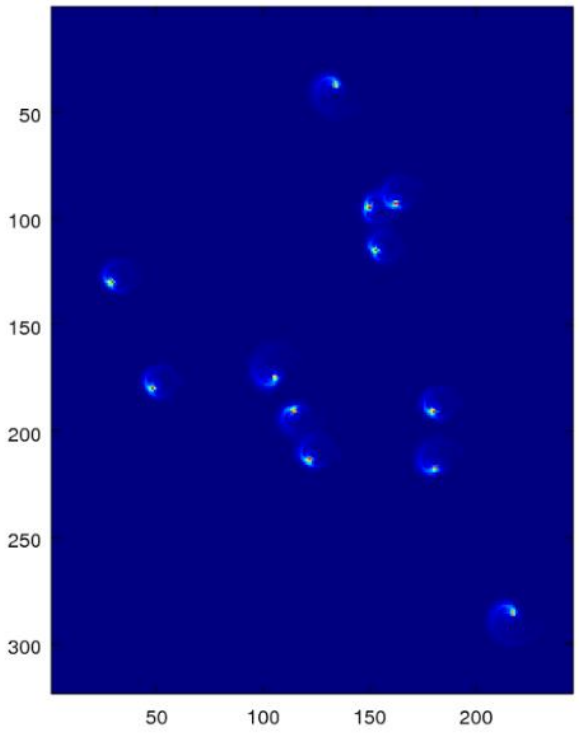

A Proposed Space Surveillance System

- An integrated radar-optical system mounted on a space asset
- Radar for debris ("swarm") detection, at > 1 km distance, with poor 3D resolution/localization
- Rotating PSF optical telescope cued, in turn, by radar for < 1 km ranges
  * Active illuminator turned on cue
  * Extend to multi-spectral system for material characterization
  ➔ Higher 3D resolution/localization and classification of debris via a sequence of snapshots
- Subsequent avoidance/kill/de-orbit maneuver initiation

Ongoing Effort

- Generalize recovery to "center" and "size" partially resolved debris for simple shapes
- Perform complete simulation-based recovery of a crowded 3D field of sources
- Design computationally efficient algorithms for near real-time performance
- Statistical characterizations for both topical areas – 3D shape and localization